Generated using the official AMS LaTeX template v6.1

Evidence for upward but not downward influence between the wintertime troposphere and stratosphere

Kara Hartig,[a] Nili Harnik,[b] and Eli Tziperman,[c,d]

[a] *Department of Physics, Harvard University, Cambridge, Massachusetts*
[b] *Department of Geosciences, Tel Aviv University, Tel Aviv, Israel*
[c] *Department of Earth & Planetary Sciences, Harvard University, Cambridge, Massachusetts*
[d] *School of Engineering and Applied Sciences, Harvard University, Cambridge, Massachusetts*

Corresponding author: Kara Hartig, kara_hartig@g.harvard.edu

ABSTRACT: Rossby waves of planetary wavenumber 1 and 2 that are excited in the troposphere can propagate upward into the stratosphere when conditions are right and disrupt the polar stratospheric vortex. It has been suggested that there is also a downward propagation that allows stratospheric vortex disruptions to influence surface weather conditions, which could improve weather forecast lead times. However, the past few decades of work on stratosphere-troposphere teleconnections have been unable to reach a consensus on either the time scale or consequences for weather of upward and downward propagation. In an attempt to identify significant patterns of covariance between the surface and stratosphere without imposing an expected pattern or timescale, we apply Maximum Covariance Analysis (MCA) with a variable time lag between pairs of tropospheric and stratospheric fields. Using over 60 years of ERA5 reanalysis for Northern Hemisphere winters, we apply MCA by calculating the singular value decomposition of the covariance matrix between a variety of surface and stratospheric fields at time lags up to seven weeks in either direction to pick out the patterns corresponding to the largest covariance between the surface and the stratosphere. We find that the greatest covariance occurs when the surface precedes the stratosphere by about one week, with little evidence of ensuing downward propagation. The dominant mode corresponding to this one-week lag is not quite the Northern Annular Mode, but something else.

1. Introduction

Compared to the troposphere, which is agitated by convection, surface forcings, and dynamic variability on all spatial scales, the stratosphere has fewer sources of variability. Dynamic variability in the extratropical stratosphere is strongly dominated on the seasonal scale by the formation and breakdown of the stratospheric polar vortex, which forms in the winter hemisphere, and on the sub-seasonal scale by infrequent but dramatic disruptions of that vortex during Sudden Stratospheric Warmings (SSWs; Andrews et al. 1987; Butler et al. 2015; Baldwin et al. 2021). While the upward influence of the troposphere on the stratosphere is well-established, it has also been suggested that the stratosphere, even with its much lower mass, is in turn capable of substantially influencing surface weather through downward propagation. But in spite of significant effort, the characteristics and mechanisms of downward propagation are still not completely understood. Our aim is to identify the time scales and spatial patterns that characterize teleconnections, both upward and downward, between stratospheric and tropospheric fields using Maximum Covariance Analysis.

SSWs are the most dramatic evidence of the *upward* influence of the surface on the stratosphere. When the eastward zonal wind in the wintertime stratosphere drops below a critical speed, planetary waves of low wavenumber excited in the troposphere can continue to propagate upward into the stratosphere (Charney and Drazin 1961). When these waves break and deposit momentum in a wave-mean flow interaction (Matsuno 1971; McIntyre and Palmer 1984; Plumb 2010), they decelerate the polar jet, resulting in a positive feedback that allows more waves to propagate upward and subsequently break, further decelerating the jet. This wave breaking feedback can lead to an SSW: a displacement, split, or collapse of the polar vortex that increases stratospheric temperatures over the pole by 40 °C or more in a matter of days (Andrews et al. 1987; Butler et al. 2015; Kidston et al. 2015; Labitzke and Kunze 2009). SSWs occur roughly six times per decade in the Northern Hemisphere (Butler et al. 2015) but have an outsized impact on the stratosphere, as the resultant temperature and wind anomalies can take over a month to return to the background state (Limpasuvan et al. 2004). Surface precursors to SSWs have been identified that are consistent with the mechanism of upward propagation of wavenumbers 1 and 2, including blocking (Quiroz 1986; Andrews et al. 1987; Martius et al. 2009) and sea level pressure or geopotential height anomalies (Ambaum and Hoskins 2002; Garfinkel et al. 2010; Kolstad et al. 2010; Lehtonen and

Karpechko 2016; Domeisen et al. 2020). But the presence of these precursors does not consistently lead to SSWs (Martius et al. 2009), motivating recent work emphasizing the importance of the stratospheric state in addition to tropospheric wave activity in generating SSWs (Birner and Albers 2017).

The mechanisms and consequences of *downward* propagation between the polar stratosphere and the troposphere are not as well-established. The strongest line of evidence for a downward influence appears in changes to the northern annular mode (NAM), which explains a large fraction of the variance in the extratropical circulation and is defined by the first empirical orthogonal function of wintertime geopotential height at a given pressure (Baldwin 2001; Thompson and Wallace 2001). Baldwin and Dunkerton (2001) used composites of 90-day low-pass filtered NAM anomalies following SSWs to identify what appeared to be a downward propagation of the negative NAM phase from the stratosphere to the surface over the course of two to three weeks, a result which subsequent studies have successfully replicated (Mitchell et al. 2013; Sigmond et al. 2013; Hitchcock and Simpson 2014), although Hitchcock and Simpson (2014) point out that the signal in the troposphere is marginal at the 95% level. The two phases of the NAM correspond to significant differences in storminess and cold air outbreaks (Marshall et al. 2001; Thompson and Wallace 2001; Hurrell et al. 2003), implying that SSWs could influence surface weather by propagating a negative NAM phase to the surface (Scaife et al. 2005; Kidston et al. 2015; Lee et al. 2019). But the conclusion of downward propagation is complicated by the results of Plumb and Semeniuk (2003), which demonstrated that the *appearance* of downward propagation from the stratosphere can be achieved even when the anomaly at each level is in fact produced by an upward influence from the lower boundary.

Progressing from the impact of SSWs on the NAM to an impact on surface weather extremes has introduced additional uncertainty. The best agreement across studies identifies a warm surface air temperature anomaly over the Labrador Sea and cooling over northern Russia on the order of 1–3 K one to two months after an SSW (Thompson et al. 2002; Kolstad et al. 2010; Lehtonen and Karpechko 2016; Ayarzagüena et al. 2020). However, there is little consensus on the temperature response over populated mid-latitude coastal areas, and even less that holds across multiple data sets or models and is statistically significant. Taking North America (away from the Labrador Sea) as an example, some studies have found an overall cold anomaly (Thompson et al. 2002), an increase in the number of cold days (Zhang et al. 2020; Thompson et al. 2002), or an increase in the area experiencing anomalously cold temperatures (Yu et al. 2018) following SSWs, while others find no significant signal or disagreement across models and with reanalysis (Lehtonen and Karpechko 2016; Ayarzagüena et al. 2020). The implications for surface weather are further complicated by the possibility of multiple sub-types of SSWs with distinct surface responses which are washed out in the average. For example, Mitchell et al. (2013) found that displacement SSWs, in which the vortex is shifted off the pole, have a distinct surface temperature response from split SSWs, in which the vortex divides into two smaller vortices, but others have found little difference when separating by event type (Lehtonen and Karpechko 2016; Charlton and Polvani 2007; White et al. 2020). The sensitivity to the design of each study could indicate that the surface signal is too weak or varies widely from one SSW to another, in which case it may be of little interest for extreme weather prediction. But it could also mean that the time window or SSW sub-type classifications used so far are not a good representation of the important dynamics, in which case an analysis method that does not presuppose either a specific time lag or stratospheric dynamical feature is desirable, such as the one we will pursue below.

Looking ahead towards the end of the 21st century, there remains much uncertainty regarding the role that climate change will have in both upward and downward propagation. Some GCMs predict more frequent SSWs in the future (Kim et al. 2017; Schimanke et al. 2013; Bell et al. 2010; Charlton-Perez et al. 2008), but these results are not conclusive and often vary across models (Butchart et al. 2000; McLandress and Shepherd 2009; Mitchell et al. 2012; Ayarzagüena et al. 2018, 2020; Rao and Garfinkel 2021), which could be the result of competing feedbacks. There is already a large natural variability among different SSWs, making it more difficult to identify a robust trend. It has been suggested, for example, that the expected strengthening of the MJO would lead to forced planetary waves that may result in more frequent SSWs (Kang and Tziperman 2017). Changes to sea ice and snow cover consistent with global warming have been associated with an observed increase in stratospheric polar vortex stretching events (Cohen et al. 2021), which are distinct from SSWs but have also been linked to cold spells over North America (Kretschmer et al. 2018a), as well as an increased likelihood that SSWs will result in cold anomalies over Canada and the midwestern US (Zhang et al. 2020). But a recent study of 12 CMIP6 models under a 4×CO_2 experiment found no significant changes in the sea level pressure response to

SSWs in most models (Ayarzagüena et al. 2020). In a much warmer climate, the negative NAM signal may become decoupled from SSWs altogether, as Hamouda et al. (2021) found that the negative Arctic Oscillation index (equivalent to NAM) following SSWs no longer propagates below the tropopause by the year 2300 under a high-emission scenario. To predict how upward and downward teleconnections will change in a warming climate, it is therefore important to identify the underlying modes of covariability.

A variety of statistical analysis methods have been employed in the search for a robust signal of downward propagation from stratospheric vortex disruptions to surface weather. Composites over many SSWs of the NAM index (Baldwin and Dunkerton 2001; Mitchell et al. 2013; Hitchcock and Simpson 2014; White et al. 2020) or surface temperature anomalies (Thompson et al. 2002; Kolstad et al. 2010; Lehtonen and Karpechko 2016; Ayarzagüena et al. 2020) are widely used. But the NAM is a hemisphere-scale feature that does not necessarily translate to consistent weather extremes in any particular region, as demonstrated above. Composites over SSWs also rely on sub-type classifications that vary across studies (Butler et al. 2015), which can lead to conflicting conclusions about the existence or pattern of a surface weather response (Mitchell et al. 2013; Lehtonen and Karpechko 2016). Clustering can identify dominant patterns within the stratosphere (Kretschmer et al. 2018b,a), but links to a surface response in clustering analysis rely on compositing rather than a direct analysis of the covariance between surface and stratosphere. Additionally, while a time lag may be applied between the stratospheric cluster and the surface, there is no obvious way to identify the optimal time lag that maximizes the covariance between the stratospheric and tropospheric fields.

We attempt to identify teleconnections between the stratosphere and the surface in winter using Maximum Covariance Analysis (MCA) (Bretherton et al. 1992; Perlwitz and Harnik 2003, 2004). MCA allows us to identify rather than impose the time scales and spatial patterns most relevant to the covariance between tropospheric and stratospheric fields. We consider all combinations of three stratospheric fields (potential vorticity, zonal wind, and vertical Eliassen-Palm flux) and three tropospheric fields (daily minimum temperature, sea level pressure, and 500 hPa geopotential height) from over 60 years of the ERA5 reanalysis product in winter. We introduce a variable time lag that offsets the stratospheric and tropospheric fields by up to ±5 weeks to find the optimal lag representing the teleconnection time scale. MCA can then identify the tropospheric and stratospheric patterns that dominate the covariance between the two fields at that optimal lag.

Time-lagged MCA offers a number of advantages over previous approaches to the study of the coupling between stratosphere and troposphere. Unlike the compositing and clustering methods described above, time-lagged MCA imposes neither a time scale nor a restriction to certain types of SSWs. Instead, an optimal time lag emerges naturally by considering the total covariance between a stratospheric field and a tropospheric field as a function of time lag. The mode patterns identified by MCA will then pick out whichever stratospheric states most strongly covary with the troposphere, during SSWs or not. MCA (and canonical correlation analysis, a close relative) has even been used to study upward and downward propagation before (Perlwitz and Graf 1995; Christiansen 2000; Perlwitz and Harnik 2003, 2004). But those studies either did not consider a time lag or focused exclusively on wave-1 and wave-2 patterns in the geopotential height, ultimately confirming that a negative NAM signal appears to lag stratospheric activity but not tying it to surface weather consequences.

Using time-lagged, MCA, we find evidence consistent with the upward stratosphere-troposphere teleconnection, with maximal covariance when the surface precedes the 10 hPa level by about one week. However, we are unable to find such evidence of downward propagation. In addition, we find that the surface pattern that accounts for the lion's share of the upward covariance with the stratosphere is neither the North Atlantic Oscillation nor the Northern Annular Mode.

2. Data & Methods

We use the ERA5 reanalysis product from 1959 to 2020 to investigate the covariance between stratospheric and tropospheric fields during Northern Hemisphere winter. On single levels, our fields include the 500 hPa geopotential height (Z500), sea level pressure (SLP), and the daily minimum surface air temperature (T_{min}). On pressure levels, we use Ertel potential vorticity (PV), zonal wind (U), and the vertical component of the Eliassen-Palm flux (EP_p) in pressure coordinates, which is calculated as follows,

$$EP_p = \frac{1}{d\bar{\theta}/dp} f a \cos\phi \, \overline{v'\theta'}, \tag{1}$$

where the overbar denotes a zonal average, f is the Coriolis parameter, a is the radius of the Earth, ϕ is latitude, $d\bar{\theta}/dp$ is the vertical derivative in pressure of the zonally-averaged potential temperature $\bar{\theta}$ calculated from daily output, and $\overline{v'\theta'}$ is the zonal average of the meridional wind anomaly $v' = v - \overline{v}$ multiplied by the potential temperature anomaly $\theta' = \theta - \overline{\theta}$. Since only the vertical component of the flux is considered in this paper, we will drop the subscript and use simply EP going forward. The use of pressure in the vertical derivative of $\overline{\theta}$ means that positive EP corresponds to downward flux and negative to upward. The variables v and θ are input at 6-hourly resolution into (1), after which EP is averaged over each day to produce daily means. All other fields are daily means calculated from hourly output except for surface temperature (daily minimums from hourly output). All fields are retrieved at $1° \times 1°$ resolution from 40°N to 90°N.

We process the data before calculating the covariance as follows. To account for the grid cell area represented by each grid point, we multiply each data field by the square root of the cosine of latitude (North et al. 1982). At each point, we remove the linear trend and the mean over the entire time span from Jan 1959 through Dec 2020. We then calculate the seasonal cycle as the day-of-year mean at each grid point, smooth the day-of-year means with a 7-day Savitzky-Golay filter of polynomial order 1 (Savitzky and Golay 1964), and subtract this smoothed seasonal cycle to convert each data field into an anomaly field. At this point, all months are included from January through December; the restriction to winter occurs in the next step while incorporating the time lag.

We introduce a time lag between the tropospheric and stratospheric fields before calculating the covariance and repeat the analysis for different lags. The analysis centers on December–February, so at a time lag of zero both the tropospheric and stratospheric anomaly fields are composed of DJF for each year in the reanalysis. To introduce a time lag of n days (positive n when troposphere lags stratosphere, negative n for troposphere leads stratosphere, for $|n|$ up to 5 weeks), we consider for each year the stratospheric field from $n/2$ days *before* Dec 1 through $n/2$ days before Feb 28, and conversely the tropospheric field from $n/2$ days *after* Dec 1 through $n/2$ days after Feb 28. In this way, a timeseries at any given point in the stratosphere is always n days before (or after, for negative n) a corresponding timeseries at any given point in the troposphere. This method maximizes the amount of time spent in DJF across both fields and allows for a variable time lag of any length and either direction in time.

To identify the relevant teleconnection time scales, we calculate the total squared covariance as a function of the time lag between a stratospheric field and a tropospheric field (Perlwitz and Harnik 2003, 2004). We start with a stratospheric anomaly field $X = X_{(MxN)}$, a matrix representing M grid points and N daily values, and a tropospheric field $Y = Y_{(LxN)}$, a matrix representing L grid points and N daily values, where each column corresponds to the spatial field on a particular day written as a vector. The cross-covariance matrix $C = C_{(MxL)}$ is then,

$$C = \frac{XY^T}{N}. \tag{2}$$

Each element of C, c_{ij}, is then the covariance over the entire timeseries between location i in X and location j in Y. The total squared covariance (often simply "total covariance" in the text that follows) between the two fields is $\sum_{i,j} c_{ij}^2$ and can be compared across time lags to determine the time lag that maximizes the covariance between the two fields. Note that, while X and Y must have the same length along the time dimension N, they need not share a spatial dimension. For example, we can calculate C when X represents the EP flux, which is solely a function of latitude, and Y is sea level pressure, which is a function of both latitude and longitude.

In order to display the total covariance between multiple pairs of fields on the same plot, it is helpful to define a normalized measure of the total covariance that makes sure the analysis results do not depend on the number of grid points nor on the variance of the fields involved. This normalized total covariance is,

$$TSC_{norm} = \frac{ML}{min(M,L)} \frac{\sum_{i,j} c_{ij}^2}{\sum_{i,n} x_{in}^2 \sum_{j,n} y_{jn}^2}. \tag{3}$$

For the case where elements of X and Y are drawn from uniform random distributions with a mean of zero, this normalized total covariance TSC_{norm} has an expectation value of 1 when $X = Y$ and approaches 0 when $X \neq Y$.

To identify the patterns in the stratosphere and the surface that best explain the covariance between the two, we apply Maximum Covariance Analysis (MCA). MCA identifies a series of pairs of patterns (modes) of the two fields that have the maximum covariance over the data time series (Bretherton et al. 1992). To apply MCA, we use singular value decomposition on the cross-covariance matrix C,

$$C = U\Sigma V^T. \tag{4}$$

This identifies a series of K mutually orthogonal modes, each characterized by a pattern in the X field (columns of $U = U_{(MxK)}$) and a corresponding pattern in the Y field (columns of $V = V_{(LxK)}$). The column vectors $\mathbf{u}_1$ and $\mathbf{v}_1$, for example, the first column of each matrix, are the most highly correlated patterns between the two fields. Note that the mode patterns $\mathbf{u}_k$ and $\mathbf{v}_k$ are agnostic to a mutual change of sign: a given mode implies simultaneously that $\mathbf{u}_k$ and $\mathbf{v}_k$ covary and that $-\mathbf{u}_k$ and $-\mathbf{v}_k$ covary. The mode patterns returned by MCA have a vector norm of 1, although when plotting these patterns we undo the latitude weighting by dividing by the square root of the cosine of latitude and thus this unit norm is not preserved in the figures that follow.

The fraction of the total covariance between the two fields that is explained by a given mode k can be determined using the corresponding singular value σ_k in the diagonal matrix Σ,

$$\begin{array}{l}\text{Fraction of covariance}\\ \text{explained by mode } k\end{array} = \frac{\sigma_k^2}{\sum_k \sigma_k^2}. \tag{5}$$

The singular values and corresponding mode patterns are ordered such that the first mode explains the largest fraction of the covariance between X and Y, $\sigma_1^2/\sum_k \sigma_k^2$, and each subsequent mode explains a progressively smaller fraction.

Once we have a set of K pairs of mode patterns, we can quantify their significance to the internal variability of fields X and Y as well. The calculations that follow can be performed on either field, so we will use X and its corresponding mode patterns $\mathbf{u}_k$ (a column vector from $U_{(MxK)}$) as an example. By projecting the original data field X onto the kth mode pattern, we define the expansion coefficient $\mathbf{a}_k = \mathbf{u}_k^T X$, which is a timeseries (a row vector) representing the strength of mode k in field X over time. If we then "reconstruct" the original data field using just that mode, we have $X_{\text{recon},k} = \mathbf{u}_k \mathbf{a}_k$. By comparing the variance of this reconstructed data field to the variance of the original data field, we can compute the fraction of the *variance* in a field explained by the corresponding mode pattern as,

$$\begin{array}{l}\text{Fraction of variance in } X\\ \text{explained by mode pattern } \mathbf{u}_k\end{array} = \frac{\sum_{i,n}(\mathbf{u}_k \mathbf{u}_k^T X)_{i,n}^2}{\sum_{i,n} x_{in}^2}. \tag{6}$$

3. Results

The following analysis is divided into three sections. Section a demonstrates the use of time-lagged MCA to search for time scales and patterns of covariance between the vertical EP flux and the sea level pressure. Section b expands this analysis to all pairs of tropospheric and stratospheric fields under consideration to identify and interpret shared time scales and covarying modes. Section c details a collection of different approaches used to investigate the possibility of downward propagation between the stratosphere and the troposphere.

a. A Demonstration of MCA for Troposphere-Stratosphere Teleconnections

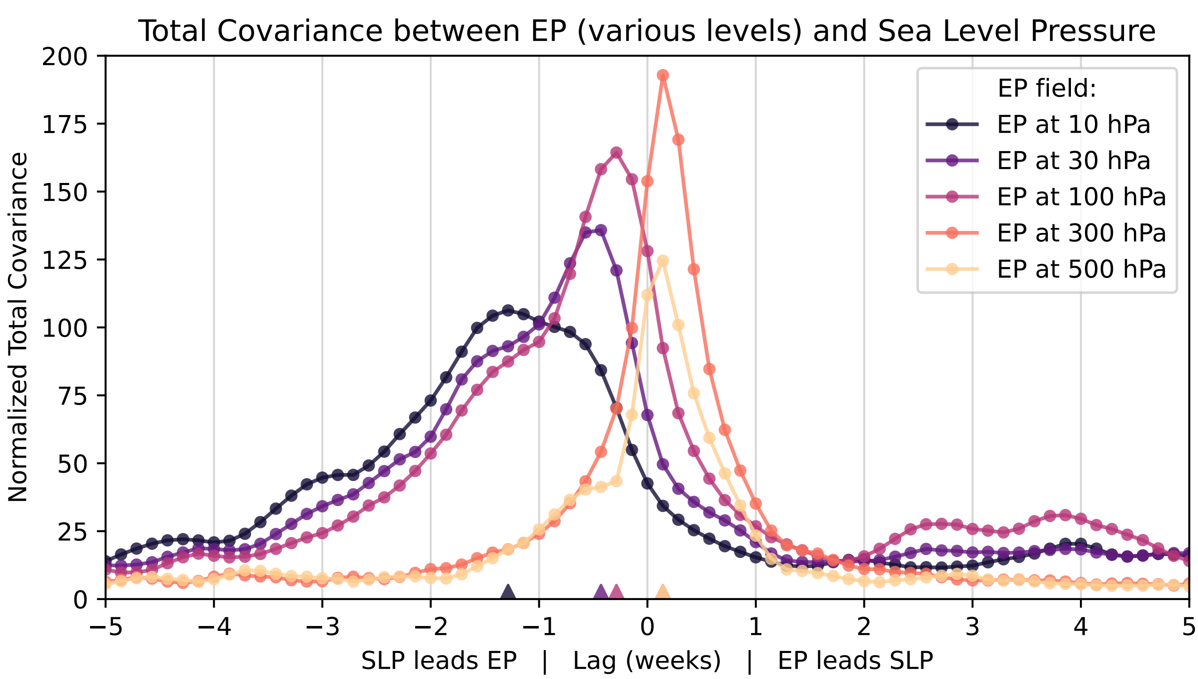

FIG. 1. **Peaks in total squared covariance pick out timescales of covariance.** The total squared covariance between sea level pressure (SLP) and the vertical component of Eliassen-Palm flux at multiple pressure levels (EP) as a function of the time lag between the surface and the stratosphere. Colored triangles along the bottom show the locations of the maxima. Each curve is normalized according to Equation 3.

To identify the time scale of teleconnections between the wintertime stratosphere and troposphere, we first demonstrate that the total squared covariance as a function of lag is a suitable tool to pick out those time scales. Sea level pressure anomalies have been shown to precede major disruptions of the stratospheric polar vortex (Kolstad et al. 2010; Cohen and Jones 2011; Mitchell et al. 2013; Lehtonen and Karpechko 2016; Domeisen et al. 2020). The vertical component of Eliassen-Palm (EP) flux is know to be a useful diagnostic for upward wave propagation (Palmer 1981; Esler and Scott 2005; Dunn-Sigouin and Shaw 2015; Jucker and Reichler 2018). We therefore begin by confirming the covariance between the two in Figure 1. For EP fluxes in the stratosphere (10, 30, and 100 hPa), sea level pressure tends to lead EP flux by 2–9 days, while there is negligible lead or lag between SLP and EP fluxes in the troposphere (300 and 500 hPa). Previous studies have identified a time scale of 5–10 days for vertical propagation of planetary-scale waves from the surface to the 10 hPa level using observations (Hirota and Sato 1969; Perlwitz and Harnik 2003), correlations of time-lagged model output (Randel 1987; Christiansen 2001), and ray-tracing theory (Karoly and Hoskins 1982), which is in good agreement with our results. Both the lag and magnitude of maximal covariance also shift in a way that is consistent with upward propagation: the longest optimal lag and smallest maximal covariance occurs between the surface and 10 hPa, which are the furthest apart in space, and the lag shortens even as the covariance grows as we consider EP fluxes closer to the surface. EP flux at 500 hPa is an exception, as its covariance with the surface is smaller than at 300 hPa, but this could be due to increased noise from synoptic activity.

We follow up with MCA to identify the spatial patterns at the surface and in the stratosphere responsible for the covariance during upward propagation. Figure 2 shows the first two modes produced by MCA between the sea level pressure and EP at 10 hPa with a time lag of −9 days, the optimal lag corresponding to the largest covariance between these two fields in Figure 1. Mode 1 corresponds to a strengthening and slight northward shift of the climatological peak in EP flux centered at 65°N (Fig. 2b) and a sea level pressure dipole with one pole over Alaska and the other over Western Russia (Fig. 2e). The sea level pressure pattern of mode 1 is consistent with a documented precursor to SSWs (Kolstad et al. 2010; Lehtonen and Karpechko 2016; Domeisen et al. 2020), with a low over Alaska and the North Pacific and a high over Western Russia, which increases our confidence that MCA is able to capture established modes of covariability between the surface and the stratosphere.

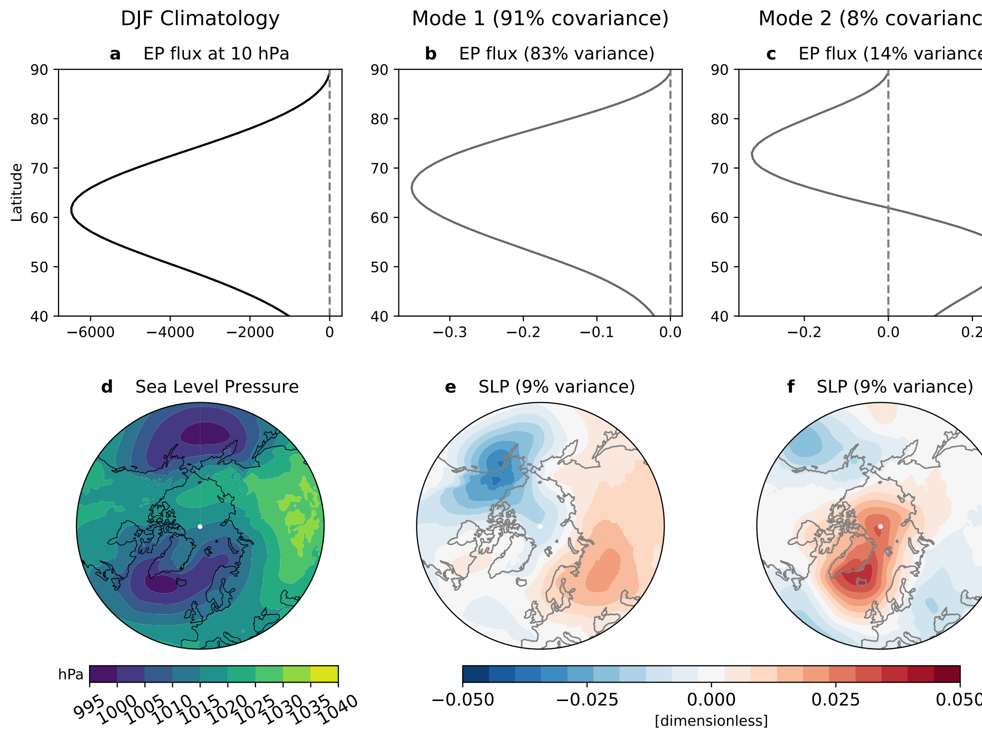

FIG. 2. **MCA identifies a known mode of covariance between the surface and stratosphere.** The climatology and first two MCA modes for EP at 10 hPa (a–c) and sea level pressure (d–f) at a time lag of −9 days (surface precedes stratosphere), corresponding to the time of maximum total covariance in Figure 1. The percent of the total covariance that is explained by each mode (Equation 5) is shown in parentheses at the top, while the percent of the variance in a specific field explained by the corresponding pattern for that mode (Equation 6) is shown above each subplot. Note that a negative EP flux is directed upward in the pressure coordinates used here.

Mode 1 accounts for the overwhelming majority, 91%, of the covariance between sea level pressure and vertical EP flux at 10 hPa. But while the stratospheric part of this mode also corresponds to the lion's share of the variance within EP flux at 10 hPa (83%), the surface component accounts for only 9% of the variance in the surface. We can conclude that the sea level pressure precursor described by mode 1 is relatively rare but corresponds to a strengthening of the EP10 peak at 65°N that accounts for most of the variability in the stratosphere. Mode 2 (Figure 2c, f), which accounts for only 8% of the covariance between sea level pressure and EP10, corresponds to a north/south shift of the EP10 maximum and resembles the Northern Annular Mode (NAM) or North Atlantic Oscillation at the surface (Wallace 2000; Baldwin 2001; Thompson et al. 2003) with poles over the Icelandic Low and the North Atlantic.

b. Characterizing upward vs downward influence

In expanding our analysis to a wide variety of both stratospheric and tropospheric fields, we find that lags from a few days up to one week maximize the total covariance in almost all cases. We consider several stratospheric fields at 10 hPa, including potential vorticity (PV), zonal wind (U) and the vertical component of EP flux (EP), alongside several tropospheric fields including daily minimum surface temperature (T_{min}), sea level pressure (SLP), and the 500 hPa geopotential height (Z500). Figure 3 of the total covariance between stratospheric fields PV10, U10, and EP10 and tropospheric fields T_{min}, SLP, and Z500 shows maximum total covariance at negative lags and insignificant covariance at positive lags for almost all pairs of tropospheric and stratospheric fields. Naively, one would expect upward propagation to result in a peak at negative lags (troposphere leads stratosphere) and downward propagation to result in a peak at positive lags (troposphere lags stratosphere). These results, therefore, provide support for upward but not downward propagation.

The singular exception is U10 and sea level pressure, which has a secondary peak when the surface lags the stratosphere by +3 days (Figure 3b). Previous studies have identified downward propagation of zonal-mean zonal wind anomalies in the wintertime stratosphere (Kuroda and Kodera 1999; Christiansen 2001), but over longer timescales of weeks to months, and not in the zonally-resolved wind field we have used here. [ADD discussion of Supplemental Figure.]

Much of the interest in downward propagation in the literature is concerned with the response of temperature extremes to stratospheric disruption, as such a connection could be used to improve weather prediction lead times. However, we find little indication of a downward influence between any of our stratospheric fields and the daily minimum temperature T_{min}. Instead, T_{min} tends to lead all stratospheric fields by a few days, but the dynamical mechanism is more likely that sea level pressure, which has the largest lead time of any tropospheric field considered, is related to upward propagation while T_{min} appears to respond to the surface pressure anomalies a few days later. Indeed, we find that the pattern of T_{min} for mode 1 is consistent with the geostrophic circulation anomalies that would be induced by the sea level pressure anomalies for mode 1, with northward

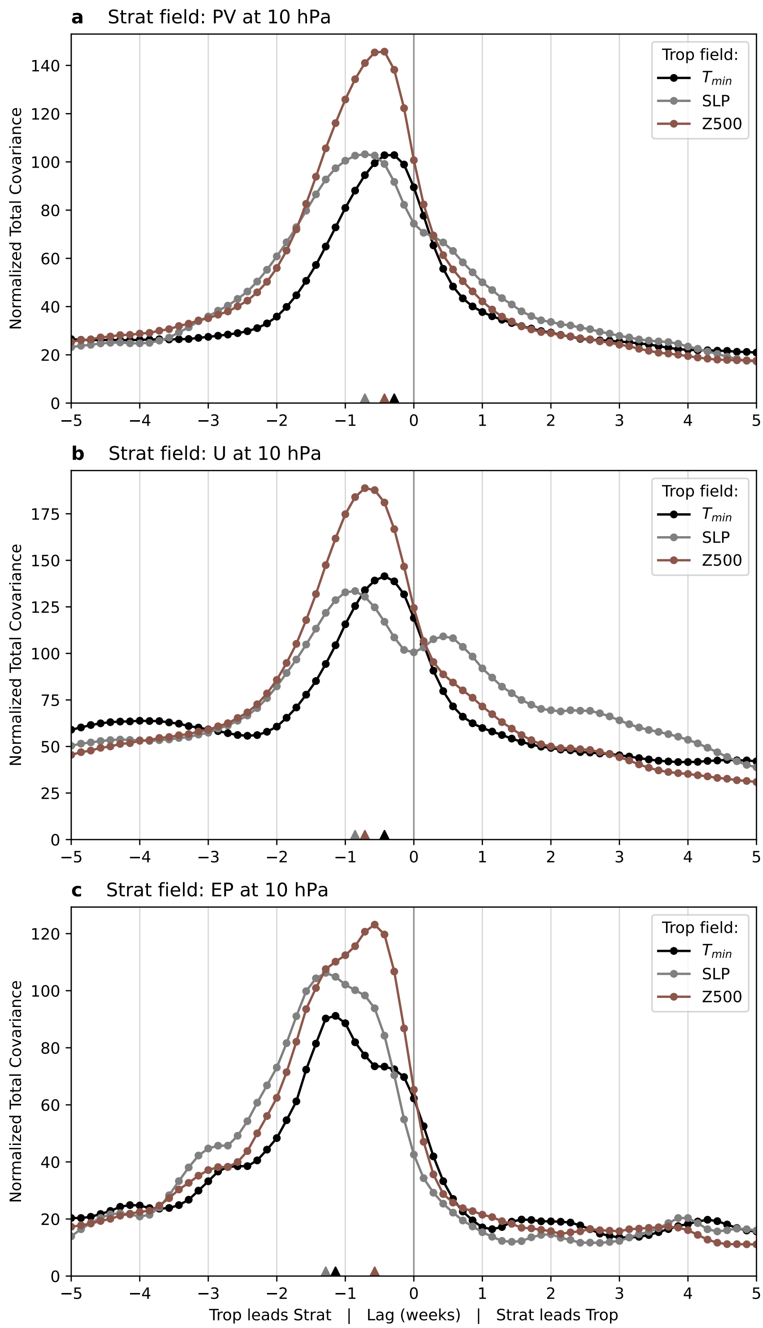

FIG. 3. **Covariance between multiple stratosphere-troposphere field pairs shows evidence for upward but not downward propagation.** Total covariance between a stratospheric field at 10 hPa (PV (a), U (b) or EP flux (c)) and a tropospheric field (daily minimum surface temperature (black), sea level pressure (grey), or 500 hPa geopotential height (brown)) as a function of the lag in weeks between the two fields. Colored triangles along the bottom show the locations of the maxima. Each curve is normalized according to Equation 3.

(warm) advection over Canada and southward (cold) over eastern Russia (see Figure S2 in the supplementary material).

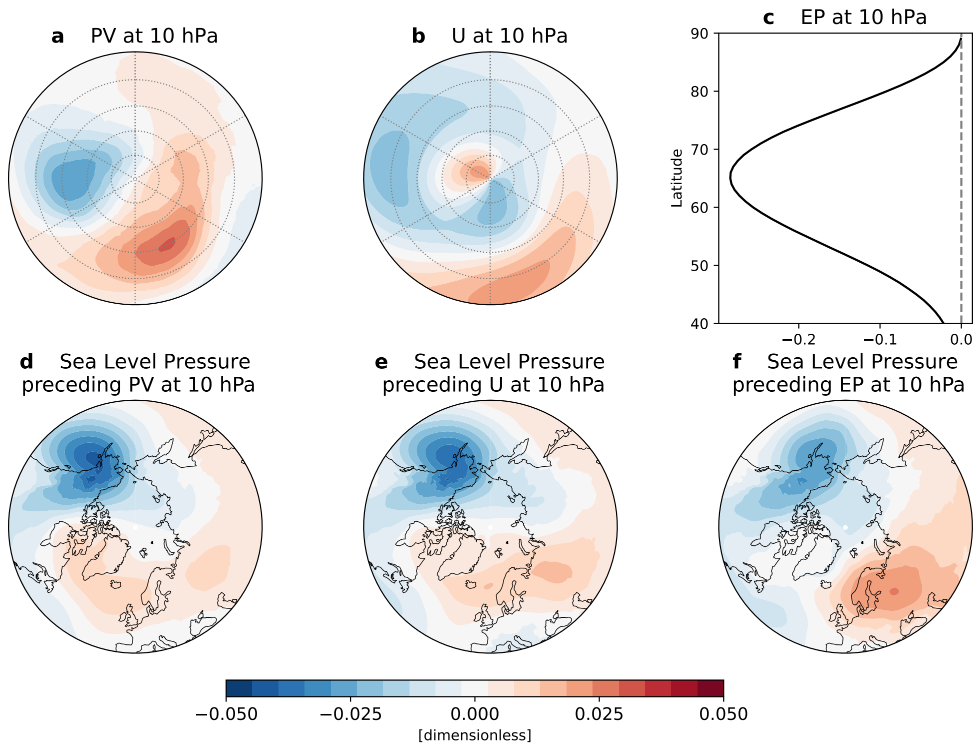

FIG. 4. **The sea level pressure anomaly that leads the stratosphere by one week is similar across different stratospheric fields and is not either the NAO or NAM/AO.** The first MCA mode between a stratospheric field at 10 hPa (PV (a), U (b), or EP flux (c)) and sea level pressure (d–f) at a lag of −1 week.

When we expand our consideration to the dominant mode across all stratospheric fields, the particular significance of the sea level pressure anomaly that we identified in Figure 2 is reinforced. Figure 4 shows the patterns corresponding to the first MCA mode across three different stratospheric fields at 10 hPa with a lag of −1 week. The sea level pressure pattern is nearly identical across all three stratospheric fields, with slight variations in the location of the pole over Eurasia. This mode indicates that a low pressure anomaly over Alaska and a high over western Russia at the surface tend to be followed a week later by: a shift of the stratospheric vortex into the sector over western Russia (4a); a clockwise circulation anomaly over western Russia and a counterclockwise anomaly over northwestern Canada in the stratosphere (4b); and a strengthening of the climatological peak

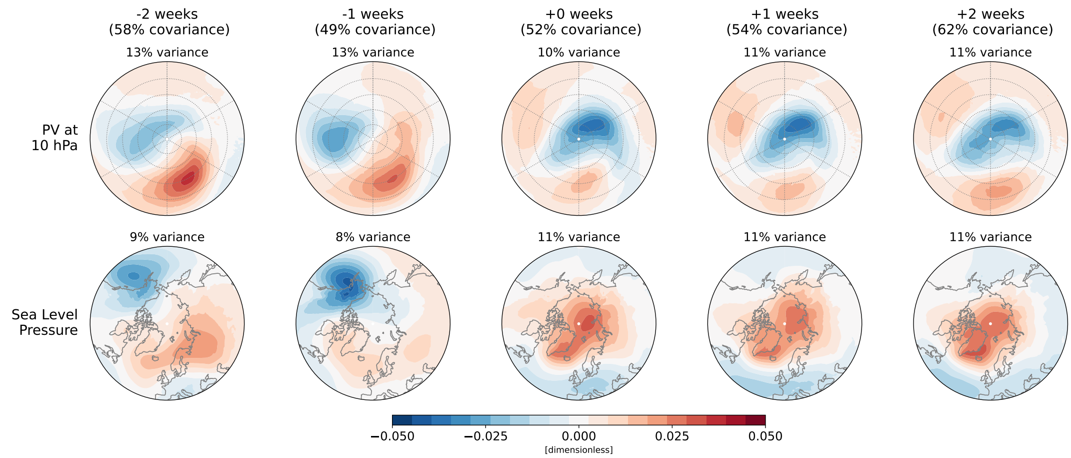

FIG. 5. **The structure of the first MCA mode changes near lag zero.** The mode pattern that maximizes covariance between PV at 10 hPa (upper row) and the sea level pressure (lower) for five different lags ranging from −2 weeks to +2 weeks.

in EP10 (4c). While there are previous studies that have identified this sea level pressure pattern as a precursor to SSWs (Kolstad et al. 2010; Lehtonen and Karpechko 2016; Domeisen et al. 2020), there are others that have found a different pattern to be more prominent (Martius et al. 2009; Kolstad et al. 2010; Mitchell et al. 2013). As our MCA analysis is not restricted to SSWs but instead considers covariance over the entire winter, one explanation for this disagreement is that the sea level pressure precursor we and others have identified is not limited to SSWs but instead describes a more general mode of covariability between the surface and the stratosphere.

We can also consider how the first mode itself changes as a function of lag between the tropospheric field (SLP) and stratospheric field (PV), illustrated in Figure 5. A major shift occurs between a lag of −1 week and no lag: the dominant mode we identified in Figure 4 subsides and is replaced by a pattern much more reminiscent of the NAM in sea level pressure (see Figure S3 in the supplementary materials for replacement of mode 1 by mode 2 just before lag zero). This NAM-like mode also persists over a large range of lags; the sea level pressure pattern that most closely covaries with PV10 at no lag also tends to lag it by +1 and even +2 weeks.

We have argued that the mode patterns at a lag of −1 week indicate upward propagation due to the corresponding peak in the total covariance at that lag. The lack of a corresponding peak in the total covariance at positive lags (Figure 3) leads us to conclude that the pattern appearing at zero and positive lags in Figure 5 is *not* an indicator of downward propagation. Our identification of a NAM-like pattern at the surface for non-negative lags is consistent with other studies that have found that a negative NAM signal at the surface tends to follow SSWs in observations (Baldwin and Dunkerton 2001; Charlton and Polvani 2007; Mitchell et al. 2013) and models (Tomassini et al. 2012; Sigmond et al. 2013; Hitchcock and Simpson 2014; White et al. 2020). However, the decrease in the total covariance as the lag increases from zero (Figure 3a) leads us to suspect that the NAM-like pattern at the surface tends to co-occur with stratospheric variability rather than lag it. If the patterns corresponding to mode 1 tend to persist for a week or two, the same pattern could remain the dominant mode even at large lags when the covariance itself is small, giving the appearance of downward propagation. We further note that the PV anomaly of mode 1 at positive lags is consistent with a split-type SSW, placing daughter vortices over Northern Europe and western Canada, which was found by Mitchell et al. (2013) to lead to a negative NAM signal at the surface where displacement-type SSWs did not. Figure 5 implies that composites following split-type SSWs may pick out a NAM-like signal in sea level pressure because it co-occurs with the SSW and then persists for a few weeks rather than because it is a result of downward propagation.

c. The Search for Downward Propagation

After failing to identify evidence of downward propagation in the MCA analysis above, we pursued a series of more targeted searches that are laid out in this section. First, composites of the vertical component of EP flux relative to SSW onset are presented in part 1. Motivated by those results, part 2 conducts an MCA analysis on EP fields that have been masked to preserve only upward or downward flux anomalies. Finally, part 3 returns to full EP fields but focuses on only the times immediately preceding or following SSWs.

1) Composites of SSWs

Downward propagation from the stratosphere to the troposphere and potentially the surface is thought to occur following SSWs. We begin with a series of composites over all SSWs in our data set (identified from the zonal-mean zonal wind reversal criterion in Charlton and Polvani (2007)) of the EP flux at various pressure levels in Figure 6. At 100 hPa, there is a dramatic decline in the upward (negative) EP flux once the SSWs begin, marked by the vertical grey line in the plot. Such

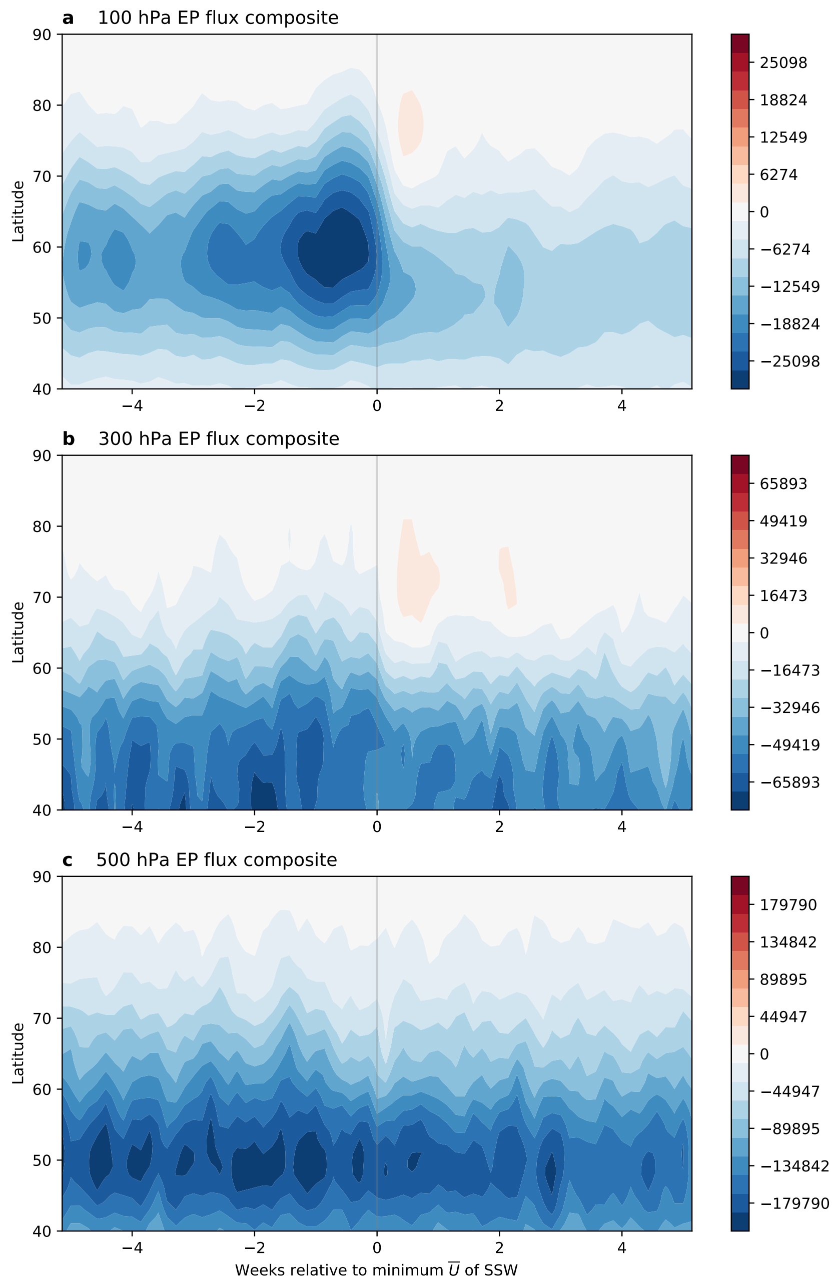

FIG. 6. **An SSW signal is visible in upper EP flux levels but disappears in the lower troposphere.** Composites over all SSWs of the vertical component of EP flux at 100 hPa (a), 300 hPa (b), and 500 hPa (c). The date of minimum zonal-mean zonal wind following SSW detection corresponds to zero along the x-axis and is indicated with a vertical grey line.

a decline could indicate the failure of planetary waves to continue to propagate upwards, a direct result of the brief window of westward zonal wind that accompanies an SSW (Charney and Drazin 1961), or the presence of downward EP flux characteristic of a downward wave propagation, or both. However, by the time we reach the mid-troposphere at 500 hPa in panel (c), any effect of the SSWs is no longer obvious to the eye. Evidently we cannot rely solely on visual detection and composites to identify a downward propagation signature following SSWs.

2) Downward EP flux

The lack of evidence for a downward propagation signal in the above analysis leads us to attempt to separate upward from downward EP prior to calculating the covariance. [Explain masking method here: discuss positive vs negative anomalies, also the caveats that this isn't exactly upward vs downward etc; reason we aren't masking both levels is because there are so few data points left that the plots become just noise].

Figure 7 shows the covariance between positive-anomaly or negative-anomaly EP at 100 hPa and the total EP at levels both above and below. There is evidence of upward propagation in Figure 7a: EP below 100 hPa tends to lead that level (brown lines peak at positive lags) while EP above 100 hPa tends to lag (purple lines peak at negative lags). The magnitude of maximum covariance varies with the vertical separation between the two fields (paler shades have higher magnitude than darker shades). Noting that the peak for EP at 850 hPa occurs about 5 days before the peak for 10 hPa, one might conclude that it takes about 5 days for upward EP flux anomalies to be communicated between 850 and 10 hPa. This time scale is consistent with Dunn-Sigouin and Shaw (2015), who found a lag of 5–10 days between heat flux anomalies in the mid-troposphere and the 10 hPa level during upward wave propagation.

Downward propagation is not as evident in Figure 7b. For downward propagation, we would expect each curve to peak in the reverse order with respect to lag that they did for upward EP: 10 and 30 hPa would peak at negative lags and 300, 500 and 850 hPa at positive lags. Instead, there are peaks at both positive and negative lags for 10, 30, and 300 hPa while 500 and 850 hPa have no peaks distinguishable from the noise. This difficulty highlights a limitation of the vertical component of EP flux anomalies: we are unable to distinguish between, for example, a weakening of upward EP flux and the presence of downward EP flux. The conflation of the two may help

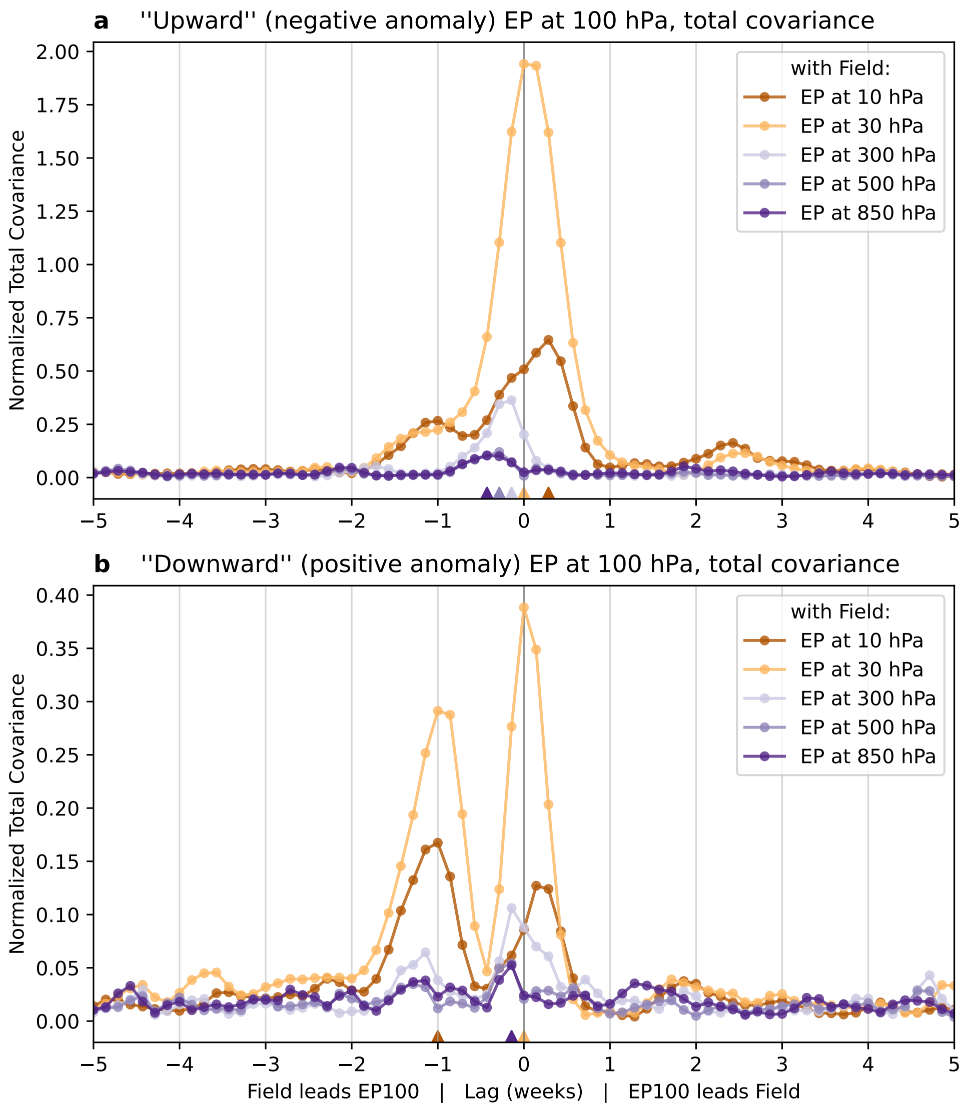

416 FIG. 7. **Total covariance can track upward but not downward propagation with positive and negative EP flux anomalies.** Total covariance between "upward" (negative EP flux, anomaly greater than 2 standard deviations) or "downward" (positive anomaly) EP flux at 100 hPa and total EP flux at various levels throughout the troposphere and stratosphere. Brown lines correspond to levels above EP100 while purple indicates levels below EP100. Colored triangles along the bottom show the locations of the maxima. Each curve is normalized according to Equation 3.

444 explain the presence of peaks at both positive and negative lags in Figure 7b. The upward EP flux signal is likely cleaner than the downward because upward wave propagation dominates the

time series and provides many more data points. A valiant attempt, but perhaps our dataset is insufficient for separating upward from downward EP flux directly and another method would be preferable.

3) EP Following SSWs

Rather than incorporate all winter days into our analysis, we now restrict our analysis to only those times corresponding to SSWs and look for downward propagation in these better-studied periods. We first identify all major SSWs between 1959 and 2020 in the ERA5 dataset using the zonal-mean zonal wind at 60°N criterion of Charlton and Polvani (2007). For each SSW, we restrict the stratospheric field to the 6 weeks following SSW onset, then apply a lag relative to that 6-week window to get a corresponding tropospheric time series. By combining these 6-week windows for all SSWs, we produce new timeseries that can be used to calculate the total covariance between the troposphere and stratosphere focused on the period during and after SSWs. Note that the same processing was applied to each data set before selecting out the SSWs as was described in section 2: at each grid point, apply area-weighting, remove the linear trend, and subtract off the seasonal cycle. For reference, we perform the same analysis but using the 6 weeks preceding SSW onset.

Even restricted to the period following SSWs, for which the magnitude of the disruption to the stratospheric vortex gives the best reason to expect downward propagation, there is still negligible covariance between stratospheric and tropospheric fields. Figure 8 shows the total squared covariance between the EP flux at 10 hPa in the 6 weeks following SSWs and EP flux at lower levels. The covariance is only significant within the stratosphere, and even there the lower levels tend to lead rather than lag EP10.

4. Conclusions

We set out to identify time lags and spatial patterns most relevant to covariance between the troposphere and stratosphere in Northern Hemisphere winter. We consider the total covariance as a function of the time lag between a set of tropospheric and stratospheric fields in ERA5 reanalysis to identify the optimal time lag and search for signals of upward and downward propagation. We find that, while there is evidence of an upward influence with a time lag of about one week, we could not find evidence of a downward influence using our analysis approach. This was determined

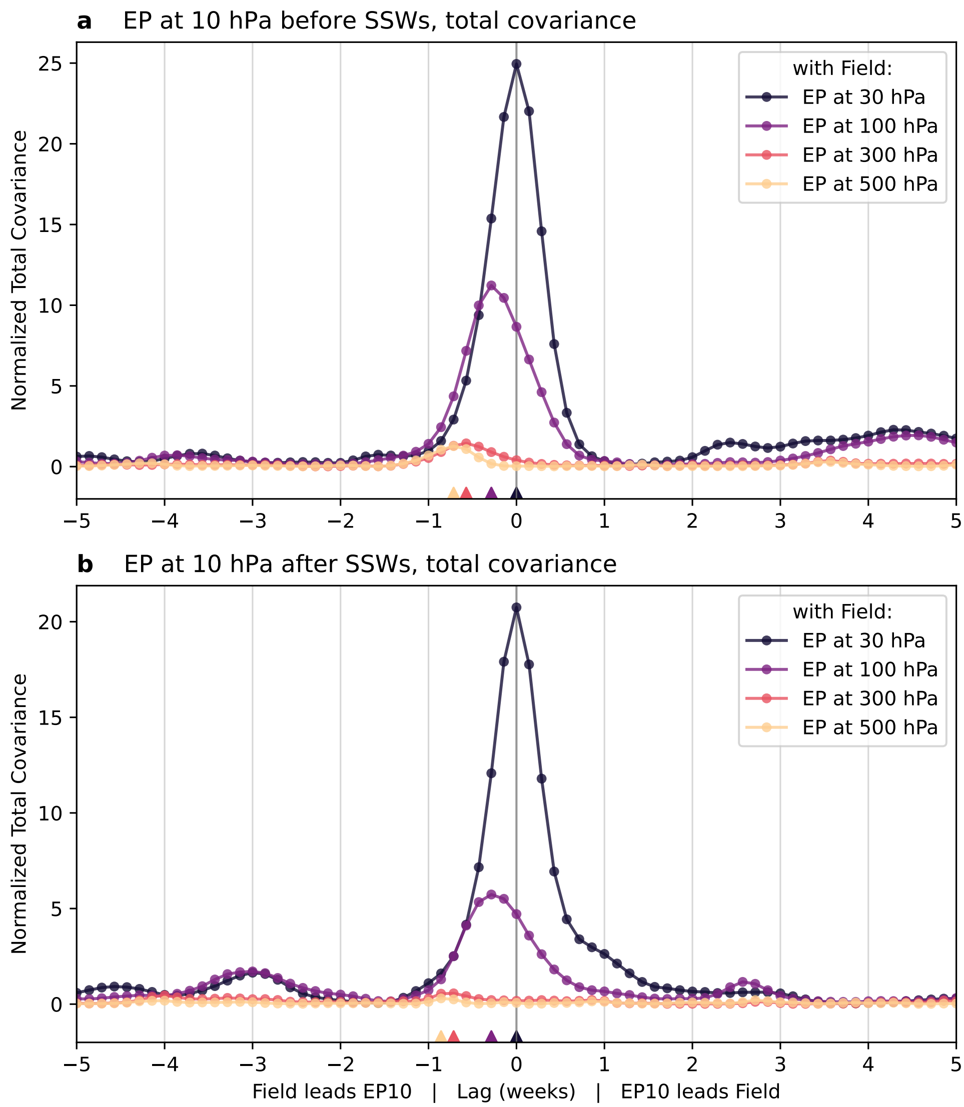

FIG. 8. **Total covariance does not pick out downward propagation even when limiting data to the window around SSWs.** Total covariance between EP at 10 hPa as the stratospheric field and EP at lower levels as a function of lag, restricting the stratospheric field to only the 6-week periods before (a) or after (b) SSWs. Colored triangles along the bottom show the locations of the maxima. Each curve is normalized according to Equation 3.

using daily ERA5 output spanning 61 years of Ertel potential vorticity, zonal wind, and the vertical component of EP flux at various pressure levels to represent the stratosphere and daily minimum surface temperature, sea level pressure, and the 500 hPa geopotential height to represent the troposphere. The covariance between all pairs of fields is maximized when the tropospheric field leads the 10 hPa field by up to one week (with a shorter lag when the same tropospheric field is paired with a lower stratospheric field). A lag of one week is in good agreement with previous studies, which have identified an upward wave propagation speed of roughly 5 km/day (Hirota and Sato 1969; Karoly and Hoskins 1982; Randel 1987) and a corresponding time scale of 5–10 days between the surface and the 10 hPa level (Christiansen 2001; Perlwitz and Harnik 2003). At the optimal time lag, we employ Maximum Covariance Analysis to identify the spatial patterns that account for the covariance between the two fields. This allows us to identify a sea level pressure pattern that accounts for the majority of the time-lagged covariance with all three stratospheric fields, featuring a pressure anomaly over Alaska and another of the opposite sign over western Russia. Some studies have identified a similar pattern as a precursor to SSWs (Kolstad et al. 2010; Lehtonen and Karpechko 2016; Domeisen et al. 2020), but it is unclear why this specific pattern is most favorable to stratospheric vortex disruptions. Our identified sea level pressure precursor is not, for example, aligned with the climatology. Such an alignment with the climatology for the 500 hPa geopotential height, for example, has been suggested as a potential mechanism for enhancing upward wave activity (Garfinkel et al. 2010; Smith and Kushner 2012).

A number of caveats are important to keep in mind when interpreting these results. Reanalysis data can be noisy for some fields due to short term variability. The time record of 61 winters is also somewhat short, particularly relative to the size of the spatial dimension (fields defined on a latitude-longitude grid have 18,000 spatial points compared to around 5,500 time points) and especially when limiting our analysis to times with positive or negative anomalies as in the upward and downward EP flux analysis in section b. While it is common practice to use SVD on datasets with more spatial samples than temporal samples, the cross-covariance matrices that result are an approximation (Bretherton et al. 1992). In addition, the mode patterns identified with MCA are symmetric with respect to sign, such that the mode pattern represented by the vectors $\mathbf{u}_k$, $\mathbf{v}_k$ necessarily implies a covariance between $-\mathbf{u}_k$ and $-\mathbf{v}_k$ as well. This may not be a desirable feature; if the processes regulating covariance between the troposphere and stratosphere are not symmetric in this way, then MCA may be incapable of identifying their effects.

Unlike many studies of stratosphere-troposphere teleconnections, our analysis is applied to the entire record rather than restricted to the times around SSWs. It has still been convenient to compare our identified mode patterns (Figures 2, 4, 5) to patterns described in the literature on

SSW precursors because they have been widely studied. Yet the fact that the sea level pressure pattern that we found to precede stratospheric variability matches the literature in some (Kolstad et al. 2010; Lehtonen and Karpechko 2016; Domeisen et al. 2020) but not all (Cohen and Jones 2011; Mitchell et al. 2013) cases may indicate that this is a stratosphere-troposphere teleconnection mode that includes but is not limited to SSWs. The expansion coefficients for the first and second MCA modes, indicating the strength of those modes at a given point in time, might serve as an index for coupling strength between the troposphere and stratosphere that avoids the ambiguities of identifying and classifying SSWs. Future work could determine the extent to which the mode patterns identified in Figure 4 describe non-SSW teleconnections at work between the troposphere and the stratosphere in Northern Hemisphere winter.

Acknowledgments. This work was funded by the U.S. Department of Energy (DOE) Office of Science Biological and Environmental Research grant DE-SC0023134. ET thanks the Weizmann Institute for its hospitality during parts of this work. XX ADD NDSEG, Cheyenne

Data availability statement.

References

Ambaum, M. H. P., and B. J. Hoskins, 2002: The NAO Troposphere–Stratosphere Connection. *Journal of Climate*, **15 (14)**, 1969–1978.

Andrews, D., J. Holton, and C. Leovy, 1987: *Middle Atmosphere Dynamics*. Academic Press, 489 pp.

Ayarzagüena, B., and Coauthors, 2018: No robust evidence of future changes in major stratospheric sudden warmings: a multi-model assessment from CCMI. *Atmospheric Chemistry and Physics*, **18 (15)**, 11 277–11 287, https://doi.org/10.5194/acp-18-11277-2018.

Ayarzagüena, B., and Coauthors, 2020: Uncertainty in the Response of Sudden Stratospheric Warmings and Stratosphere-Troposphere Coupling to Quadrupled CO2 Concentrations in CMIP6 Models. *Journal of Geophysical Research: Atmospheres*, **125 (6)**, e2019JD032 345, https://doi.org/10.1029/2019JD032345.

Baldwin, M. P., 2001: Annular modes in global daily surface pressure. *Geophysical Research Letters*, **28 (21)**, 4115–4118, https://doi.org/10.1029/2001GL013564.

Baldwin, M. P., and T. J. Dunkerton, 2001: Stratospheric harbingers of anomalous weather regimes. *Science*, **294 (5542)**, 581–4.

Baldwin, M. P., and Coauthors, 2021: Sudden Stratospheric Warmings. *Reviews of Geophysics*, **59 (1)**, e2020RG000 708, https://doi.org/10.1029/2020RG000708.

Bell, C. J., L. J. Gray, and J. Kettleborough, 2010: Changes in Northern Hemisphere stratospheric variability under increased CO_2 concentrations. *Quarterly Journal of the Royal Meteorological Society*, **136 (650)**, 1181–1190, https://doi.org/10.1002/qj.633.

Birner, T., and J. R. Albers, 2017: Sudden Stratospheric Warmings and Anomalous Upward Wave Activity Flux. *Sola*, **13A (Special_Edition)**, 8–12, https://doi.org/10.2151/sola.13A-002.

Bretherton, C. S., C. Smith, and J. M. Wallace, 1992: An Intercomparison of Methods for Finding Coupled Patterns in Climate Data. *Journal of Climate*, **5 (6)**, 541–560, https://doi.org/10.1175/1520-0442(1992)005<0541:AIOMFF>2.0.CO;2.

Butchart, N., J. Austin, J. R. Knight, A. A. Scaife, and M. L. Gallani, 2000: The response of the stratospheric climate to projected changes in the concentrations of well-mixed greenhouse gases from 1992 to 2051. *Journal of Climate*, **13 (13)**, 2142–2159, https://doi.org/10.1175/1520-0442(2000)013<2142:TROTSC>2.0.CO;2.

Butler, A. H., D. J. Seidel, S. C. Hardiman, N. Butchart, T. Birner, and A. Match, 2015: Defining Sudden Stratospheric Warmings. *Bulletin of the American Meteorological Society*, **96 (11)**, 1913–1928, https://doi.org/10.1175/BAMS-D-13-00173.1.

Charlton, A. J., and L. M. Polvani, 2007: A New Look at Stratospheric Sudden Warmings. Part I: Climatology and Modeling Benchmarks. *Journal of Climate*, **20 (3)**, 449–469, https://doi.org/10.1175/JCLI3996.1.

Charlton-Perez, A. J., L. M. Polvani, J. Austin, and F. Li, 2008: The frequency and dynamics of stratospheric sudden warmings in the 21st century. *Journal of Geophysical Research*, **113 (D16)**, D16 116, https://doi.org/10.1029/2007JD009571.

Charney, J. G., and P. G. Drazin, 1961: Propagation of planetary-scale disturbances from the lower into the upper atmosphere. *Journal of Geophysical Research (1896-1977)*, **66 (1)**, 83–109, https://doi.org/10.1029/JZ066i001p00083.

Christiansen, B., 2000: A model study of the dynamical connection between the Arctic Oscillation and stratospheric vacillations. *Journal of Geophysical Research: Atmospheres*, **105 (D24)**, 29 461–29 474, https://doi.org/10.1029/2000JD900542.

Christiansen, B., 2001: Downward propagation of zonal mean zonal wind anomalies from the stratosphere to the troposphere: Model and reanalysis. *Journal of Geophysical Research: Atmospheres*, **106 (D21)**, 27 307–27 322, https://doi.org/10.1029/2000JD000214.

Cohen, J., L. Agel, M. Barlow, C. I. Garfinkel, and I. White, 2021: Linking Arctic variability and change with extreme winter weather in the United States. *Science*, **373 (6559)**, 1116–1121, https://doi.org/10.1126/science.abi9167.

Cohen, J., and J. Jones, 2011: Tropospheric Precursors and Stratospheric Warmings. *Journal of Climate*, **24 (24)**, 6562–6572, https://doi.org/10.1175/2011JCLI4160.1.

Domeisen, D. I. V., and Coauthors, 2020: The Role of the Stratosphere in Subseasonal to Seasonal Prediction: 2. Predictability Arising From Stratosphere-Troposphere Coupling. *Journal of Geophysical Research: Atmospheres*, **125 (2)**, e2019JD030 923, https://doi.org/10.1029/2019JD030923.

Dunn-Sigouin, E., and T. A. Shaw, 2015: Comparing and contrasting extreme stratospheric events, including their coupling to the tropospheric circulation. *Journal of Geophysical Research: Atmospheres*, **120 (4)**, 1374–1390, https://doi.org/10.1002/2014JD022116.

Esler, J. G., and R. K. Scott, 2005: Excitation of Transient Rossby Waves on the Stratospheric Polar Vortex and the Barotropic Sudden Warming. *Journal of the Atmospheric Sciences*, **62 (10)**, 3661–3682, https://doi.org/10.1175/JAS3557.1.

Garfinkel, C. I., D. L. Hartmann, and F. Sassi, 2010: Tropospheric Precursors of Anomalous Northern Hemisphere Stratospheric Polar Vortices. *Journal of Climate*, **23 (12)**, 3282–3299, https://doi.org/10.1175/2010JCLI3010.1.

Hamouda, M. E., C. Pasquero, and E. Tziperman, 2021: Decoupling of the Arctic Oscillation and North Atlantic Oscillation in a warmer climate. *Nature Climate Change*, **11 (2)**, 137–142, https://doi.org/10.1038/s41558-020-00966-8.

Hirota, I., and Y. Sato, 1969: Periodic variation of the winter stratospheric circulation and intermittent vertical propagation. *Journal of the Meteorological Society of Japan. Ser. II*, **47 (5)**, 390–402, https://doi.org/10.2151/jmsj1965.47.5_390.

Hitchcock, P., and I. R. Simpson, 2014: The Downward Influence of Stratospheric Sudden Warmings. *Journal of the Atmospheric Sciences*, **71 (10)**, 3856–3876, https://doi.org/10.1175/JAS-D-14-0012.1.

Hurrell, J. W., Y. Kushnir, G. Ottersen, and M. Visbeck, 2003: An overview of the North Atlantic Oscillation. *Geophysical Monograph Series*, J. W. Hurrell, Y. Kushnir, G. Ottersen, and M. Visbeck, Eds., Vol. 134, American Geophysical Union, Washington, D. C., 1–35, https://doi.org/10.1029/134GM01.

Jucker, M., and T. Reichler, 2018: Dynamical Precursors for Statistical Prediction of Stratospheric Sudden Warming Events. *Geophysical Research Letters*, **45 (23)**, 13,124–13,132, https://doi.org/10.1029/2018GL080691.

Kang, W., and E. Tziperman, 2017: More Frequent Sudden Stratospheric Warming Events due to Enhanced MJO Forcing Expected in a Warmer Climate. *Journal of Climate*, **30 (21)**, 8727–8743, https://doi.org/10.1175/JCLI-D-17-0044.1.

Karoly, D. J., and B. J. Hoskins, 1982: Three dimensional propagation of planetary waves. *Journal of the Meteorological Society of Japan. Ser. II*, **60 (1)**, 109–123.

Kidston, J., A. A. Scaife, S. C. Hardiman, D. M. Mitchell, N. Butchart, M. P. Baldwin, and L. J. Gray, 2015: Stratospheric influence on tropospheric jet streams, storm tracks and surface weather. *Nature Geoscience*, **8 (6)**, 433–440, https://doi.org/10.1038/ngeo2424.

Kim, J., S.-W. Son, E. P. Gerber, and H.-S. Park, 2017: Defining Sudden Stratospheric Warming in Climate Models: Accounting for Biases in Model Climatologies. *Journal of Climate*, **30 (14)**, 5529–5546, https://doi.org/10.1175/JCLI-D-16-0465.1.

Kolstad, E. W., T. Breiteig, and A. A. Scaife, 2010: The association between stratospheric weak polar vortex events and cold air outbreaks in the Northern Hemisphere. *Quarterly Journal of the Royal Meteorological Society*, **136 (649)**, 886–893, https://doi.org/10.1002/qj.620.

Kretschmer, M., J. Cohen, V. Matthias, J. Runge, and D. Coumou, 2018a: The different stratospheric influence on cold-extremes in Eurasia and North America. *npj Climate and Atmospheric Science*, **1 (1)**, 1–10, https://doi.org/10.1038/s41612-018-0054-4.

Kretschmer, M., D. Coumou, L. Agel, M. Barlow, E. Tziperman, and J. Cohen, 2018b: More-Persistent Weak Stratospheric Polar Vortex States Linked to Cold Extremes. *Bulletin of the American Meteorological Society*, **99 (1)**, 49–60, https://doi.org/10.1175/BAMS-D-16-0259.1.

Kuroda, Y., and K. Kodera, 1999: Role of planetary waves in the stratosphere-troposphere coupled variability in the northern hemisphere winter. *Geophysical Research Letters*, **26 (15)**, 2375–2378, https://doi.org/10.1029/1999GL900507.

Labitzke, K., and M. Kunze, 2009: On the remarkable Arctic winter in 2008/2009. *Journal of Geophysical Research: Atmospheres*, **114 (D1)**, https://doi.org/10.1029/2009JD012273.

Lee, S. H., J. C. Furtado, and A. J. Charlton-Perez, 2019: Wintertime North American Weather Regimes and the Arctic Stratospheric Polar Vortex. *Geophysical Research Letters*, **46 (24)**, 14 892–14 900, https://doi.org/10.1029/2019GL085592.

Lehtonen, I., and A. Y. Karpechko, 2016: Observed and modeled tropospheric cold anomalies associated with sudden stratospheric warmings. *Journal of Geophysical Research: Atmospheres*, **121 (4)**, 1591–1610, https://doi.org/10.1002/2015JD023860.

Limpasuvan, V., D. W. J. Thompson, and D. L. Hartmann, 2004: The Life Cycle of the Northern Hemisphere Sudden Stratospheric Warmings. *Journal of Climate*, **17 (13)**, 2584–2596, https://doi.org/10.1175/1520-0442(2004)017<2584:TLCOTN>2.0.CO;2.

Marshall, J., and Coauthors, 2001: North Atlantic climate variability: phenomena, impacts and mechanisms. *International Journal of Climatology*, **21 (15)**, 1863–1898, https://doi.org/10.1002/joc.693.

Martius, O., L. M. Polvani, and H. C. Davies, 2009: Blocking precursors to stratospheric sudden warming events. *Geophysical Research Letters*, **36 (14)**, https://doi.org/10.1029/2009GL038776.

Matsuno, T., 1971: A Dynamical Model of the Stratospheric Sudden Warming. *Journal of the Atmospheric Sciences*, **28 (8)**, 1479–1494, https://doi.org/10.1175/1520-0469(1971)028<1479:ADMOTS>2.0.CO;2.

McIntyre, M. E., and T. N. Palmer, 1984: The 'surf zone' in the stratosphere. *Journal of Atmospheric and Terrestrial Physics*, **46 (9)**, 825–849, https://doi.org/10.1016/0021-9169(84)90063-1.

McLandress, C., and T. G. Shepherd, 2009: Impact of climate change on stratospheric sudden warmings as simulated by the Canadian middle atmosphere model. *Journal of Climate*, **22 (20)**, 5449–5463, https://doi.org/10.1175/2009JCLI3069.1.

Mitchell, D. M., L. J. Gray, J. Anstey, M. P. Baldwin, and A. J. Charlton-Perez, 2013: The Influence of Stratospheric Vortex Displacements and Splits on Surface Climate. *Journal of Climate*, **26 (8)**, 2668–2682, https://doi.org/10.1175/JCLI-D-12-00030.1.

Mitchell, D. M., S. M. Osprey, L. J. Gray, N. Butchart, S. C. Hardiman, A. J. Charlton-Perez, and P. Watson, 2012: The effect of climate change on the variability of the northern hemisphere stratospheric polar vortex. *Journal of the Atmospheric Sciences*, **69 (8)**, 2608–2618, https://doi.org/10.1175/JAS-D-12-021.1.

North, G. R., T. L. Bell, R. F. Cahalan, and F. J. Moeng, 1982: Sampling Errors in the Estimation of Empirical Orthogonal Functions. *Monthly Weather Review*, **110 (7)**, 699–706, https://doi.org/10.1175/1520-0493(1982)110<0699:SEITEO>2.0.CO;2.

Palmer, T. N., 1981: Aspects of stratospheric sudden warmings studied from a transformed Eulerian-mean viewpoint. *Journal of Geophysical Research: Oceans*, **86 (C10)**, 9679–9687, https://doi.org/10.1029/JC086iC10p09679.

Perlwitz, J., and H.-F. Graf, 1995: The Statistical Connection between Tropospheric and Stratospheric Circulation of the Northern Hemisphere in Winter. *Journal of Climate*, **8 (10)**, 2281–2295, https://doi.org/10.1175/1520-0442(1995)008<2281:TSCBTA>2.0.CO;2.

Perlwitz, J., and N. Harnik, 2003: Observational Evidence of a Stratospheric Influence on the Troposphere by Planetary Wave Reflection. *Journal of Climate*, **16 (18)**, 3011–3026, https://doi.org/10.1175/1520-0442(2003)016<3011:OEOASI>2.0.CO;2.

Perlwitz, J., and N. Harnik, 2004: Downward Coupling between the Stratosphere and Troposphere: The Relative Roles of Wave and Zonal Mean Processes. *Journal of Climate*, **17 (24)**, 4902–4909, https://doi.org/10.1175/JCLI-3247.1.

Plumb, R. A., 2010: Planetary Waves and the Extratropical Winter Stratosphere. *The Stratosphere: Dynamics, Transport, and Chemistry*, **190**, 23–41.

Plumb, R. A., and K. Semeniuk, 2003: Downward migration of extratropical zonal wind anomalies. *Journal of Geophysical Research: Atmospheres*, **108 (D7)**, https://doi.org/10.1029/2002JD002773.

Quiroz, R. S., 1986: The association of stratospheric warmings with tropospheric blocking. *Journal of Geophysical Research: Atmospheres*, **91 (D4)**, 5277–5285, https://doi.org/10.1029/JD091iD04p05277.

Randel, W. J., 1987: A Study of Planetary Waves in the Southern Winter Troposphere and Stratosphere. Part I: Wave Structure and Vertical Propagation. *Journal of the Atmospheric*

Sciences, **44 (6)**, 917–935, https://doi.org/10.1175/1520-0469(1987)044<0917:ASOPWI>2.0.CO;2.

Rao, J., and C. I. Garfinkel, 2021: CMIP5/6 models project little change in the statistical characteristics of sudden stratospheric warmings in the 21st century. *Environmental Research Letters*, **16 (3)**, 034 024, https://doi.org/10.1088/1748-9326/abd4fe.

Savitzky, A., and M. J. E. Golay, 1964: Smoothing and Differentiation of Data by Simplified Least Squares Procedures. *Analytical Chemistry*, **36 (8)**, 1627–1639, https://doi.org/10.1021/ac60214a047.

Scaife, A. A., J. R. Knight, G. K. Vallis, and C. K. Folland, 2005: A stratospheric influence on the winter NAO and North Atlantic surface climate. *Geophysical Research Letters*, **32 (18)**, https://doi.org/10.1029/2005GL023226.

Schimanke, S., T. Spangehl, H. Huebener, and U. Cubasch, 2013: Variability and trends of major stratospheric warmings in simulations under constant and increasing GHG concentrations. *Climate Dynamics*, **40 (7-8)**, 1733–1747, https://doi.org/10.1007/s00382-012-1530-x.

Sigmond, M., J. F. Scinocca, V. V. Kharin, and T. G. Shepherd, 2013: Enhanced seasonal forecast skill following stratospheric sudden warmings. *Nature Geoscience*, **6 (2)**, 98–102, https://doi.org/10.1038/ngeo1698.

Smith, K. L., and P. J. Kushner, 2012: Linear interference and the initiation of extratropical stratosphere-troposphere interactions. *Journal of Geophysical Research: Atmospheres*, **117 (D13)**, https://doi.org/10.1029/2012JD017587.

Thompson, D. W. J., M. P. Baldwin, and J. M. Wallace, 2002: Stratospheric Connection to Northern Hemisphere Wintertime Weather: Implications for Prediction. *Journal of Climate*, **15 (12)**, 1421–1428, https://doi.org/10.1175/1520-0442(2002)015<1421:SCTNHW>2.0.CO;2.

Thompson, D. W. J., S. Lee, and M. P. Baldwin, 2003: Atmospheric Processes Governing the Northern Hemisphere Annular Mode/North Atlantic Oscillation. *The North Atlantic Oscillation: Climatic Significance and Environmental Impact*, American Geophysical Union (AGU), 81–112, https://doi.org/10.1029/134GM05.

Thompson, D. W. J., and J. M. Wallace, 2001: Regional climate impacts of the Northern Hemisphere annular mode. *Science*, **293 (5527)**, 85–9.

Tomassini, L., E. P. Gerber, M. P. Baldwin, F. Bunzel, and M. Giorgetta, 2012: The role of stratosphere-troposphere coupling in the occurrence of extreme winter cold spells over northern Europe. *Journal of Advances in Modeling Earth Systems*, **4 (4)**, https://doi.org/https://doi.org/10.1029/2012MS000177.

Wallace, J. M., 2000: North atlantic oscillatiodannular mode: Two paradigms—one phenomenon. *Quarterly Journal of the Royal Meteorological Society*, **126 (564)**, 791–805, https://doi.org/10.1002/qj.49712656402.

White, I. P., C. I. Garfinkel, E. P. Gerber, M. Jucker, P. Hitchcock, and J. Rao, 2020: The Generic Nature of the Tropospheric Response to Sudden Stratospheric Warmings. *Journal of Climate*, **33 (13)**, 5589–5610, https://doi.org/10.1175/JCLI-D-19-0697.1.

Yu, Y., M. Cai, C. Shi, and R. Ren, 2018: On the Linkage among Strong Stratospheric Mass Circulation, Stratospheric Sudden Warming, and Cold Weather Events. *Monthly Weather Review*, **146 (9)**, 2717–2739, https://doi.org/10.1175/MWR-D-18-0110.1.

Zhang, P., Y. Wu, G. Chen, and Y. Yu, 2020: North American cold events following sudden stratospheric warming in the presence of low Barents-Kara Sea sea ice. *Environmental Research Letters*, **15 (12)**, 124 017, https://doi.org/10.1088/1748-9326/abc215.